ADVANCED FUNCTIONAL MATERIALS
www.afm-journal.de

www.MaterialsViews.com

Precise Tuning of $(YBa_2Cu_3O_{7-\delta})_{1-x}$:$(BaZrO_3)_x$ Thin Film Nanocomposite Structures

Run Zhao, Weiwei Li, Joon Hwan Lee, Eun Mi Choi, Yan Liang, Wei Zhang, Rujun Tang, Haiyan Wang, Quanxi Jia, Judith L. MacManus-Driscoll, and Hao Yang**

Self-assembled nanocomposite films and coatings have huge potential for many functional and structural applications. However, control and manipulation of the nanostructures is still at very early stage. Here, guidelines are established for manipulating the types of composite structures that can be achieved. In order to do this, a well studied $(YBa_2Cu_3O_{7-\delta})_{1-x}$:$(BaZrO_3)_x$ 'model' system is used. A switch from $BaZrO_3$ nanorods in $YBa_2Cu_3O_{7-\delta}$ matrix to planar, horizontal layered plates is found with increasing x, with a transitional cross-ply structure forming between these states at $x = 0.4$. The switch is related to a release in strain energy which builds up in the $YBa_2Cu_3O_{7-\delta}$ with increasing x. At $x = 0.5$, an unusually low strain state is observed in the planar composite structure, which is postulated to arise from a pseudo-spinodal mechanism.

1. Introduction

Both "top-down" lithography and "bottom-up" self-assembly methods are used to fabricate nanostructures. As the technology is pushed to ever-smaller length scales, lithography becomes increasingly challenging. Simple and cost-effective self-assembly processes have attracted tremendous attention for creating a range of nanoscale structure types.[1,2] For example, self-assembly has been successfully demonstrated in copolymers, membranes, and proteins.[3–6] In general, great strides have been made in organic systems but with very limited progress in inorganic systems.[7,8] On the other hand, the area of metal oxide electronics is growing rapidly because of the exciting prospects for next generation devices in data processing and storage.[9–11] Additionally, tremendous application possibilities exist by employing nanocomposite oxides in functional systems, e.g. those incorporating superconductors, solar cells, ferroelectrics, multiferroics, metamaterials, colloidal matter, and biosensors etc.[4–8,12–18] Exciting possibilities also exist in structural systems, e.g. coatings for wear resistance and in smart materials.[19–21] However, while considerable work has been undertaken over the last 20 years to understand self-assembly of semiconductor quantum dots in thin films, including understanding of long range elastic interactions and strain effects, much less has been studied for oxide films.[22–26] We now need to be able to dial in the precise structure so as to give novel functionalities by interaction or coupling between the constituents.[8,12,13]

So far, in the $(YBa_2Cu_3O_{7-\delta})_{1-x}$:$(BaZrO_3)_x$ system, the focus has been on low x (typically <0.2), since for these values improved flux pinning properties are obtained.[27–38] Here, we study this system further to investigate how wide ranges of the x value ($x = 0.05$, 0.15, 0.25, 0.4, and 0.5) influence the forms of nanocomposite structure. A complete understanding of the problem would require full knowledge of the thermodynamics of the system, knowing precise interfacial energies of all interfaces in the system in three dimensions. This includes knowing the elastic constants of the constituents in three dimensions. Without the availability of this information, we can only use assumptions about the different interfacial energy terms which need to be considered. Hence, here we apply a simple strain energy balance for the vertical nanorod versus horizontal plate structures observed. We make assumptions about interfacial energies based both on experimental observations and on considering relative magnitudes of values for the two different structures. From this analysis, we are able to understand why in the $(YBa_2Cu_3O_{7-\delta})_{1-x}$:$(BaZrO_3)_x$ system a switch occurs from vertical nanorod to horizontal plate nanostructure, and we predict in which other nanocomposite systems this is likely to occur.

R. Zhao, W. Li, Y. Liang, W. Zhang, Dr. R. Tang, Prof. H. Yang
School of Physical Science and Technology
& Collaborative Innovation Center of Suzhou Nano Science and Technology
Soochow University
Suzhou 215006, China
E-mail: yanghao@suda.edu.cn
J. H. Lee, Prof. H. Wang
Department of Electrical and Computer Engineering
Texas A&M University
College Station
Texas 77843-3128, USA
Dr. Q. X. Jia
Center for Integrated Nanotechnologies
Los Alamos National Laboratory
Los Alamos
New Mexico 87545, USA
E. M. Choi, Prof. J. L. MacManus-Driscoll
Department of Materials Science and Metallurgy
University of Cambridge
Cambridge, CB2 3QZ, UK
E-mail: jld35@cam.ac.uk

DOI: 10.1002/adfm.201304302

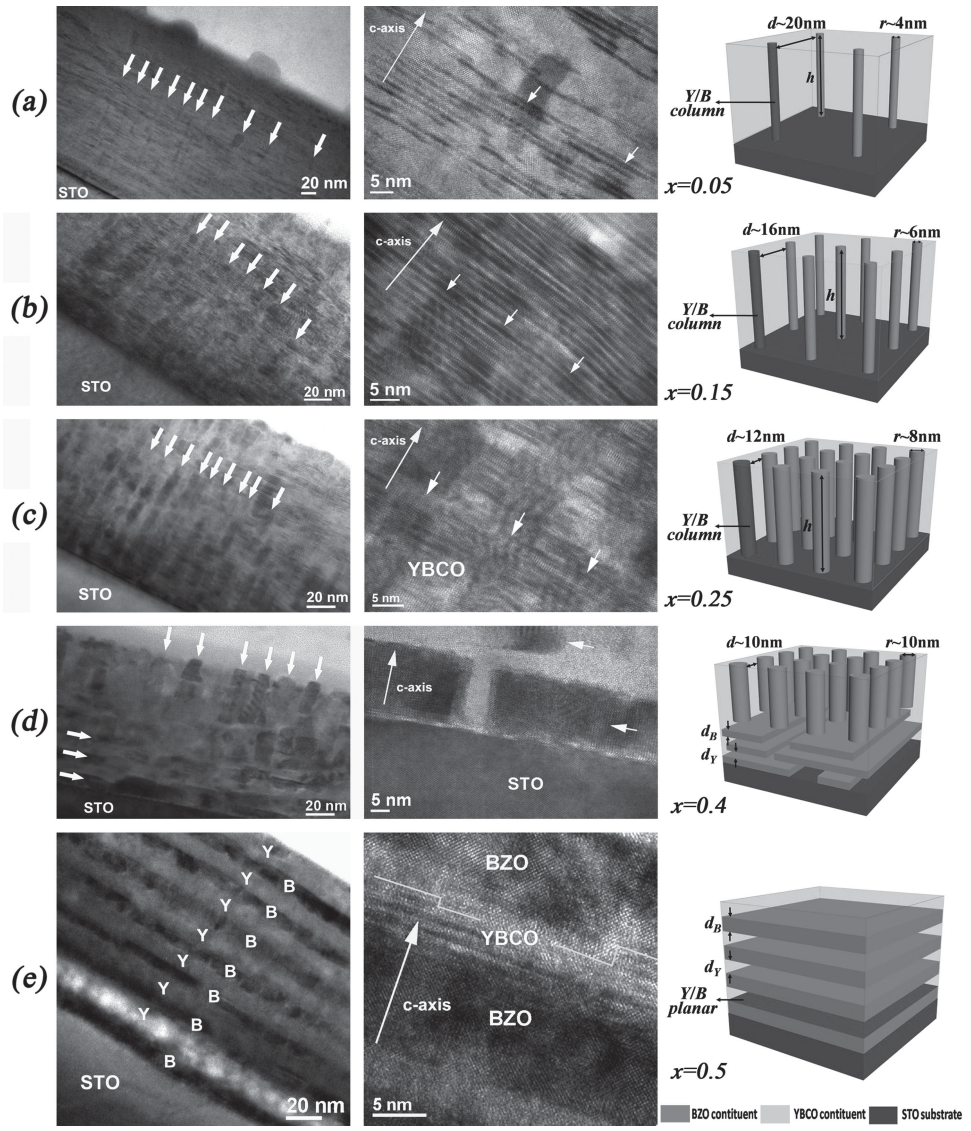

Figure 1. Cross-sectional TEM images of YBCO:BZO thin films with compositions of x = (a) 0.05, (b) 0.15, (c) 0.25, (d) 0.4, and (e) 0.5. The bright and dark contrasts correspond to the YBCO and BZO, respectively. The BZO nanocolumns or nanolayers are marked by white arrows. In figure (e), Y and B represent YBCO and BZO respectively. The white lines indicate the interface steps. The corresponding schematic diagrams for these compositions are shown on the right panel. The radius of BZO nanocolumn (r), the nanocolumn separation (d), the length of BZO nanocolumn (h), and the thicknesses of YBCO (d_Y) and BZO (d_B) layers have been indicated in the schematic diagrams. Both d_Y and d_B have a value of ~10 ± 2 nm. The interface between BZO column and YBCO matrix $\begin{pmatrix} Y/B \\ column \end{pmatrix}$ and the interface between BZO and YBCO layers $\begin{pmatrix} Y/B \\ planar \end{pmatrix}$ have also been shown in the schematic diagrams.

2. Results and Discussion

2.1. Experimental Observations of Nanocomposite Structural Forms

Figure 1a–e show cross-sectional transmission electron microscopy (TEM) images of $(YBa_2Cu_3O_{7-\delta})_{1-x}$:$(BaZrO_3)_x$ (YBCO:BZO) films with compositions of x = 0.05, 0.15, 0.25, 0.4, and 0.5. The low-magnification, high-resolution, and schematic images are shown as left, middle, and right panel respectively. A vertical nanocolumnar structure of BZO in a YBCO matrix is observed for x < 0.4, consistent with the widely reported results on YBCO thin films with low molar ratio inclusion of BZO.[27–31,34] The vertical nanocolumnar structure forms instead of random BZO nanoparticles because the strain fields around existing nanoparticles lead to a lower nucleation energy for new nanoparticles.[23] A change from vertical columnar structure to a horizontal multilayered structure occurs at x > 0.4. As indicated on the right panel images, the radii of the BZO nanocolumns (r) increase on average from 4 to 10 nm with increasing x from 0.05 to 0.4. At the same time, the nanocolumn separation (d) decreases from ~20 nm at x = 0.05 to ~10 nm at x = 0.4. As we discuss later, the reduction in d is critical to generate large strains in the YBCO as the distance available for strain

relaxation by misfit dislocations decreases laterally between the columns.

At the transition composition of $x \sim 0.4$, a unique hybrid, cross-ply nanostructure comprised of both horizontal plates at the base, and vertical columns at the top, exists. We note that this intriguing new structure has never been demonstrated before in thin films. It is particularly interesting because it could have wide structural applications (e.g. optimizing materials to be hard and stiff in all directions),[39,40] as well as functional applications (e.g. creating flux pinning centers in all angular directions in superconductors).[30,41] Perhaps more interestingly is the possibility to create composite thin films which are optimized both in terms of structural and functional properties (e.g. for smart, sensing films which are also strong, chemically stable, etc.). One could, for example, envision a new generation of electronic leak detecting waste containment materials or a thermal protective coating on an engine part which is also an energy harvesting device. In fact, while such duality of functions is limited in the man-made world, such self-assembled structural/functional materials exist in nature already, e.g. optical effects in strong, stiff butterfly wings and beetle shells, and chemoreceptors in structurally optimized receptors in animals and fishes.[42–46]

For $x = 0.5$, a pure spontaneously ordered, multilayered structure is formed with a perfect BZO/YBCO sequence up to a micro-meter scale. Both the YBCO and BZO layers have a thickness of ~10 ± 2 nm. From the HRTEM image of Figure 1e (central image), we can see there is a semi-coherent interface between YBCO and BZO with some misfit dislocations and interface steps. Because of these interfacial defects, the in-plane strain between YBCO and BZO is partially relaxed. Selected area diffraction (SAD) images (not shown) indicate the epitaxial orientation relations to be $(001)_{YBCO}\|(001)_{BZO}$ and $[010]_{YBCO}\|[010]_{BZO}$, which is consistent with the results from X-ray diffraction (XRD) measurements. **Figure 2** shows a typical XRD θ–2θ scan of one of the films ($x = 0.25$). As expected,[27,33]

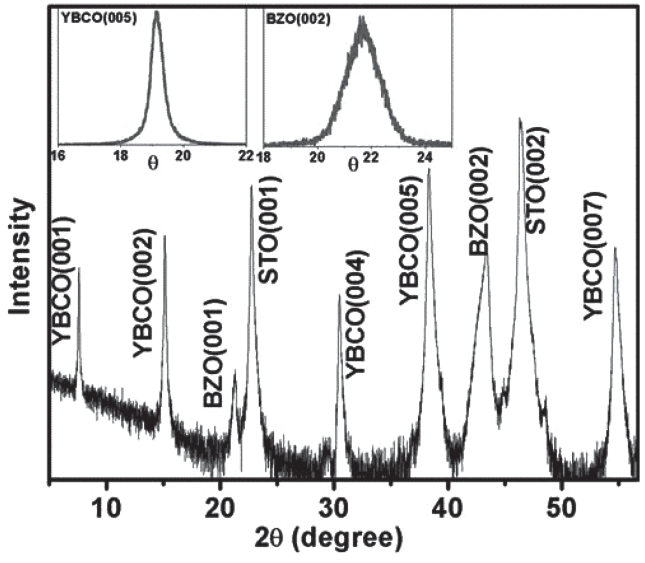

Figure 2. XRD θ–2θ scan of a YBCO:BZO thin film with $x = 0.25$. The insets show rocking curves of YBCO (005) and BZO (002) diffraction peaks.

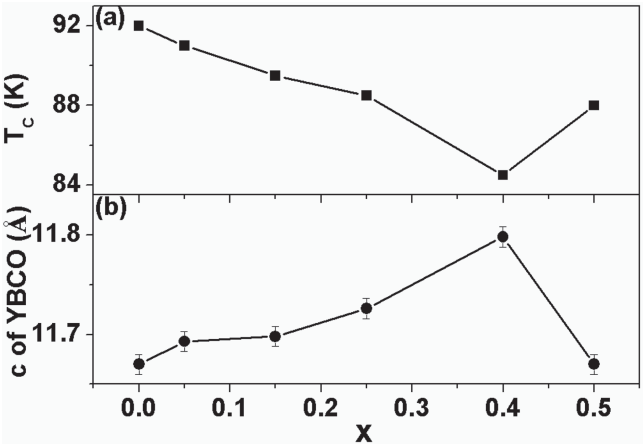

Figure 3. (a) Critical temperature (T_c) and (b) c lattice constant of YBCO phase in composite films as a function of x.

the films show only (00l) peaks of YBCO and BZO, indicative of preferential orientation of these two phases. The insets to Figure 2 show rocking curves of the YBCO (005) and BZO (002) peaks. The full-width at half-maximum (FWHM) of these two peaks are 0.44° and 1.50°, respectively, which are higher than those of pure YBCO and pure BZO films, consistent with the large lattice mismatch between the YBCO and BZO. BZO is a cubic perovskite structure with $a = 4.193$ Å, and fully oxygenated YBCO is an orthorhombic perovskite with $a = 3.819$ Å, $b = 3.886$ Å, and $c/3 \sim 3.893$ Å. Hence, the lattice mismatch values are ~8.7% and ~7.7% along in-plane and out-of-plane directions, respectively. Based on the XRD phi-scans (not shown), the in-plane alignment between each phases and the substrate can be described as $(001)_{YBCO}\|(001)_{BZO}\|(001)_{STO}$ and $[010]_{YBCO}\|[010]_{BZO}\|[010]_{STO}$, consistent with the TEM results and earlier works.[30,33]

The superconducting critical temperature (T_c) and c-axis lattice constant of YBCO in the nanocomposite films (**Figure 3**a and b, respectively) show a clear and opposite trend with x. The dependence of c on x is relatively flat for $x = 0.05$ and $x = 0.15$, but starts to increase more rapidly at $x > 0.15$. The c-lattice parameter peaks at $x = 0.4$ with an unusually high value of 11.798 ± 0.008 Å. As mentioned above, the high strain levels induced in the YBCO originate from the decreasing d values with increasing x. From $x = 0.4$ to $x = 0.5$, the value sharply decreases to 11.670 ± 0.008 Å which is close to the bulk value of fully oxygenated YBCO (11.680 Å). For the vertical nanostructured sample ($x \leq 0.4$), the results are in good general agreement with previous reports of the dependence of T_c on c-lattice constant.[47,48] However, for the $x = 0.5$ (planar structure), while the c-lattice constant is similar to that of $x = 0.0$, T_c is ~4 K lower. This is consistent with the presence of some in-plane strain induced by the planar heteroepitaxial growth of YBCO with BZO (as discussed above for Figure 1e).

2.2. Energetic Analysis of Nanocomposite Forms Depending on x

Now we turn to understanding, from energetic considerations, why, at a critical x value, the nanocomposite structure switches

from vertical to horizontal. We consider both the availability of species for forming the respective nanostructures as well as the interfacial energies involved.

Let us first consider the case of low x values (e.g. $x = 0.05$). Here there is insufficient BZO available to give planar, plate-like growth of BZO in the YBCO matrix because the influx of species from the PLD plume is too fast to allow the BZO to attach horizontally to a BZO nanoparticle. BZO grows vertically because it continues to be added to the film from the plume. After limited lateral diffusion, the BZO will preferentially nucleate either in a strained region in the YBCO matrix above the surface of a BZO particle or directly on top of a BZO particle itself.[28,31]

Then, considering higher x values, there exists the possibility that there is sufficient BZO to attach laterally to an existing BZO particle and therefore for a planar horizontal layer to grow. The precise value for this to occur will depend on growth conditions. We then need to consider the relative interface energies for either situation – columnar nanorod growth or planar horizontal growth. The full energetic considerations of both cases are shown in the supplementary section. Two key equations are arrived at:

$$\gamma_{\substack{columnar\\total}} = 2\gamma_{\substack{Y/B\\column}} \frac{V_f h}{r} + substrate + surface\ \ terms \quad (1)$$

$$\gamma_{\substack{planar\\total}} = 2\gamma_{\substack{Y/B\\planar}} \frac{V_f h}{d_B} + substrate + surface\ \ terms \quad (2)$$

where B is BZO, Y is YBCO, $\gamma_{\substack{columnar\\total}}$ is the total interface energy of the vertical nanocolumnar structure per unit area, $\gamma_{\substack{planar\\total}}$ is the total interface energy of planar structure per unit area, $\gamma_{\substack{Y/B\\column}}$ is the interface energy per unit area of BZO columns (cylinders) in YBCO matrix, $\gamma_{\substack{Y/B\\planar}}$ is the interface energy per unit area of BZO plates in YBCO, V_f is the volume fraction of BZO in YBCO, h is the length of BZO nanocolumn (in case of $x = 0.05$, 0.15, and 0.25, h is the same as the film thickness – i.e. Figures 1a-c indicate that the BZO nanocolumns extend approximately through the whole film), r is the radius of the BZO nanocolumn, and d_B is the thickness of the BZO layer in the planar structure. The substrate+surface terms are similar for both Equation (1) and (2). Also, they are of much smaller magnitude than the YBCO/BZO interfacial terms because the areas involved are much less. Hence, they can be neglected.

When $\gamma_{\substack{columnar\\total}} = \gamma_{\substack{planar\\total}}$, both the columnar and planar structures should be present simultaneously in a film. In fact, this is what we see in the $x = 0.4$ film. We also observe in the $x = 0.4$ sample that $r = d_B$, i.e. the radius of the vertical BZO nanocolumn is around the thickness of a BZO nanoplates, at ~10 nm. From Equation (1) and (2), this therefore implies that for $x = 0.4$, $\gamma_{\substack{Y/B\\column}} = \gamma_{\substack{Y/B\\planar}}$. It is now important to consider how $\gamma_{\substack{Y/B\\column}}$ varies with x (inferred from how c lattice constant of YBCO varies with x). $\gamma_{\substack{Y/B\\planar}}$ only needs to be considered when x is large enough such that the BZO planar layers can form continuously in the YBCO matrix.

For low x (e.g. 0.05), as discussed above, the columns are very fine (~4 nm in diameter) and the spacing between them is large (~20 nm) (Figure 1a). The BZO nanocolumns, which are much stiffer than the YBCO matrix (E_{BZO} and E_{YBCO} are ~256 GP_a and ~64 GP_a, respectively),[49–52] are expected to strain the YBCO in the regions close to the columns. Also, since the YBCO width between the columns is relatively large compared to critical thickness (~1–3 nm) it can partially relax. The c value of 11.693 ± 0.008 Å measured in the YBCO is consistent with this (Figure 3).

As x increases, the density of BZO columns increases and the YBCO width between the columns (d) decreases. For $x = 0.05$, 0.15, 0.25, and 0.4, d has the average value of 20, 16, 12, and 10 nm, respectively. Hence, with increasing x a larger proportion of the YBCO is strained by the BZO, and there is insufficient lateral length for it to relax. This is consistent with the observed increase in c lattice parameter of YBCO with values of 11.693 ± 0.008 Å, 11.698 ± 0.008 Å, 11.726 ± 0.008 Å, and 11.798 ± 0.008 Å, for the same range of x (Figure 3). The increase of built in strain energy in the system naturally means than $\gamma_{\substack{Y/B\\column}}$ also increases with x.

At $\boldsymbol{x = 0.4}$, the planar structure is found at the base of the film and the nanocolumnar structure is found at the top (Figure 1d). Hence, a cross-ply structure is formed. The reason for this order, i.e. planar at the bottom and nanocolumnar at the top, is likely because at this x value the plates are not yet fully continuous. The widths are ~40 nm because there is insufficient BZO available to give continuous layers and this means there is an additional energy associated with edge effects. This also leads to increased roughness with thickness and hence to an increase in $\gamma_{\substack{Y/B\\planar}}$ as the film grows, up to the point that $\gamma_{\substack{Y/B\\planar}}$ will become larger than $\gamma_{\substack{Y/B\\column}}$.

At $\boldsymbol{x > 0.4}$, in order for plates to become more stable than nanocolumns, the following inequalities must be obeyed:

$$\gamma_{\substack{columnar\\total}} > \gamma_{\substack{planar\\total}} \text{ and } 2\gamma_{\substack{Y/B\\column}} \frac{V_f h}{r} > 2\gamma_{\substack{Y/B\\planar}} \frac{V_f h}{d_B} \quad (3)$$

And so,

$$\gamma_{\substack{Y/B\\column}} \frac{1}{r} > \gamma_{\substack{Y/B\\planar}} \frac{1}{d_B} \quad (4)$$

Since at $x \sim 0.4$, r and d_B were observed to be approximately equivalent (as shown above), then for Equation (4) to be valid, $\gamma_{\substack{Y/B\\column}} > \gamma_{\substack{Y/B\\planar}}$. Indeed, it is not surprising that this is so, since the $\gamma_{\substack{Y/B\\column}}$ term increases substantially with x, as manifest by the sharp upturn in c, particularly at $x > 0.15$. We recall that at $x = 0.4$ the c value of 11.798 ± 0.008 Å is very large (Figure 3). As far as known, such an extended c parameter has not previously been obtained in thick YBCO films unless very large cation disorder was induced by non-optimal growth.[53]

To determine whether the assumption that $\gamma_{\substack{Y/B\\column}} > \gamma_{\substack{Y/B\\planar}}$ is reasonable, it is important to know whether the $\gamma_{\substack{Y/B\\planar}}$ term (assessed by measuring the in-plane strain) changes with x. Hence, we undertook x-ray reciprocal space mapping (RSM) of (108) and (018) YBCO peaks of the $x = 0.4$ and

0.5 samples. The a and b lattice parameters were calculated by using the RSM data in combination with Bragg Bretano scans. Unsurprisingly, for these nanostructured samples the RSM peaks were relatively broad, making the error bars on the measured values quite large. For $x = 0.4$, $a = 3.835 \pm 0.010$ Å, $b = 3.875 \pm 0.012$ Å. For $x = 0.5$, $a = 3.847 \pm 0.008$ Å, $b = 3.882 \pm 0.027$ Å. To within error, both samples have a axes somewhat larger than unstrained fully oxygenated YBCO values (3.819 Å) and so there is likely to be a small amount of oxygen loss for both samples. As shown before, in planar YBCO films grown on lattice mismatched substrates, oxygen loss and rearrangement occurs in the YBCO basal plane to minimise the interfacial strain.[54] Hence, $\gamma_{\substack{Y/B \\ planar}}$ will be lowered by this mechanism. It is important to note though, that there is no similar strain relieving mechanism to reduce $\gamma_{\substack{Y/B \\ column}}$ along the c direction. Hence, as x increases, $\gamma_{\substack{Y/B \\ column}}$ becomes so large (as manifest by the increasing c values) that it is energetically favourable for a switch to the planar structure to occur.

At $x = 0.5$, there is a pure horizontal plate nanostructure throughout the whole film (Figure 1e), which means Equation (4) is fully obeyed. The BZO thickness (d_B) is still low (~10 ± 2 nm), which is similar to the r value at $x = 0.4$. Hence, again, from Equation (4), $\gamma_{\substack{Y/B \\ column}} \gamma_{\substack{Y/B \\ planar}}$. It is very interesting that the c parameter of YBCO (11.670±0.008 Å) is relaxed to the bulk value. Considering the low thickness of the YBCO layer (~10 ± 2 nm) and also considering it is sandwiched between the lattice mismatched BZO layers, even with some partial stress relief from misfit dislocations (Figure 1e), the YBCO should still be highly strained. There is a ~8.7% in-plane tensile strain between the YBCO and the BZO which should cause an out-of-plane compressive strain in the YBCO, and hence to considerable shrinkage of c to conserve volume as a result of the elastic deformation. Since this is not the case, it is highly likely that pseudo-spinodal effects are playing a role. Here, the ordered plate-like nanostructure forms to minimize interfacial strain energies.[13]

In several previous nanocomposite systems we have studied, for $x = 0.5$ the vertical nanostructure forms and not the planar structure, as found here.[55,56] The main reason for the difference to previous studied systems is that different crystallographic structures were combined together before, and hence $\gamma_{\substack{Y/B \\ planar}}$ was much larger than here. In other words, in previous systems there was no possibility of semi-coherent, planar interfaces forming which is what is required for pseudo-spinodal decomposition.

2.3. Broader Outcomes and Predictions for Heteroepitaxial Nanocomposite Thin Films

The outcome of our above energetic analysis has implications for a broad range of nanocomposite films. We are able to predict that the planar horizontal structure will form when the phases in the composite have the same crystallographic structure and hence relatively low interface energies. Hence, as long as there is sufficient material available (sufficiently high x value), a planar, ordered structure will be most energetically stable. The planar ordered structure may form by pseudo-spinodal decomposition to give a semi-coherent interface or by another mechanism which can yield low interfacial energies, e.g. interfacial reconstruction or domain matching epitaxy. More work is needed to fully understand the possible mechanisms which yield low energy interfaces in oxides.

On the other hand, for a low x value, a columnar nanostructure will always form because this is limited by the availability of material. For a certain range of x values (e.g. $x = 0.4$–0.6, where continuous planar structures are able to form because there is a sufficiently high fraction of both materials), it is possible to create a cross-ply structure with both columns and horizontal plates.

When the phases in the composite have different crystallographic structures, the possibility of semi-coherent, planar interfaces forming is low, and then vertical nanocomposite structures will always form, regardless of x (at least for $x > 0.05$). Our predictions have important implications for the growing area of smart, multifunctional thin films.

3. Conclusion

We have used YBCO:BZO as a model system to realize the precise tuning of inorganic nanocomposite thin films. A nanostructure switch from vertical columnar structure to horizontal multilayered structure has been found. Coincident with this switch is a release in the strain energy of YBCO (which builds up with increasing x) occurs. A cross-ply structure comprised of horizontal layer and vertical nanocolumn was found at the transition point of $x = 0.4$. Energetic considerations were used to explain the structures which we observed. This work provides clear design guidelines for manipulating nanostructures of self-assembled oxide thin films and can easily be extended to other inorganic materials that present immediate opportunities for fabrication of controllable structures.

4. Experimental Section

The YBCO:BZO composite films were grown on (001) oriented $SrTiO_3$ (STO) substrates by pulsed laser deposition (PLD) from composite targets. Ceramic pellets with different x values were used as the targets. Deposition temperature was 820 °C and oxygen pressure was 200 mTorr. After deposition, the films were cooled down to room temperature in an oxygen pressure of 300 Torr without any further thermal treatment. The film thicknesses, revealed by transmission electron microscopy (TEM, FEI Tecnai F20 analytical microscope), were 120–200 nm. The crystal structure was investigated by X-ray diffraction (XRD, Siemens D5000 four-circle diffractometer). Bragg Bretano scans were undertaken to measure c parameters and reciprocal space maps near the YBCO (108) and (018) peaks were used (in combination with the Bragg Bretanao scans) to determine a and b lattice parameters. The superconductive critical temperature (T_c) was evaluated by both alternating current (a.c.) susceptibility and transport measurement techniques using a physical properties measurement system (PPMS-9, Quantum Design).

Supporting Information

Supporting Information is available from the Wiley Online Library or from the author.

Acknowledgements

The authors acknowledge the support of the National Natural Science Foundation of China (Grant No. 11004145, 11274237, 51202153, and 51228201), the Natural Science Foundation of Jiangsu Province under Grant No. BK2010223, the Scientific Research Foundation for the Returned Overseas Chinese Scholars (State Education Ministry of China), and the Priority Academic Program Development of Jiangsu Higher Education Institutions (PAPD). J.L.M.D gratefully acknowledges funding from the ERC Advanced Investigator Grant, Novox, ERC-2009-AFG-247276. The TEM work at Texas A&M University is funded by the US National Science Foundation (NSF-1007969 and 1401266). The work at Los Alamos was supported, in part, by the Center for Integrated Nanotechnologies, an Office of Science User Facility operated for the US Department of Energy (DOE) Office of Science. Q.X.J also acknowledges the support from the Los Alamos National Laboratory LDRD Program.

Received: December 29, 2013
Revised: March 31, 2014
Published online: June 23, 2014

[1] G. M. Whitesides, B. Grzybowski, *Science* **2002**, *295*, 2418.
[2] J. Lehn, *Science* **2002**, *295*, 2400.
[3] S. Jain, F. S. Bates, *Science* **2003**, *300*, 460.
[4] D. Lingwood, K. Simons, *Science* **2010**, *327*, 46.
[5] L. V. Schäfer, D. H. de Jong, A. Holt, A. J. Rzepiela, A. H. de Vries, B. Poolman, J. A. Killian, S. J. Marrink, *Proc. Natl. Acad. Sci. USA* **2011**, *108*, 1343.
[6] E. Edlund, O. Lindgren, M. N. Jacobi, *Phys. Rev. Lett.* **2011**, *107*, 085503.
[7] G. Kostorz, *Phase Transformations in Materials* Wiley-VCH, Germany **2001**.
[8] R. Ramesh, N. Spaldin, *Nat. Mater.* **2007**, *6*, 21.
[9] J. Mannhart, D. G. Schlom, *Science* **2010**, *327*, 1607.
[10] J. Ma, J. M. Hu, Z. Li, C. W. Nan, *Adv. Mater.* **2011**, *23*, 1062.
[11] J. Chakhalian, A. J. Millis, J. Rondinelli, *Nat. Mater.* **2012**, *11*, 92.
[12] B. S. Guiton, P. K. Davies, *Nat. Mater.* **2007**, *6*, 586.
[13] J. L. MacManus-Driscoll, *Adv. Funct. Mater.* **2010**, *20*, 2035.
[14] M. H. Zheng, F. Straub, Q. Zhan, P. L. Yang, W. K. Hsieh, F. Zavaliche, Y. H. Chu, U. Dahmen, R. Ramesh, *Adv. Mater.* **2006**, *18*, 2747.
[15] Y. Ni, W. F. Rao, A. G. Khachaturyan, *Nano. Lett.* **2009**, *9*, 3275.
[16] M. G. Blamire, J. L. MacManus-Driscoll, N. D. Mathur, Z. H. Barber, *Adv. Mater.* **2009**, *21*, 3827.
[17] K. A. Bogle, V. Anbusathaiah, M. Arredondo, J. Y. Lin, Y. H. Chu, C. O'Neill, J. M. Gregg, M. R. Castell, V. Nagarajan, *ACS Nano* **2010**, *4*, 5139.
[18] G. Decher, B. Lehr, K. Lowack, Y. Lvov, J. Schmitt, *Biosens. Bioelectron.* **1994**, *9*, 677.
[19] A. M. Díez-Pascual, M. Naffakh, C. Marco, G. Ellis, M. A. Gómez-Fatou, *Prog. Mater. Sci.* **2012**, *57*, 1106.
[20] Y. D. Liu, H. J. Choi, *Soft Matter* **2012**, *8*, 11961.
[21] V. Q. Nauyen, A. S. Ahmed, R. V. Ramanujan, *Adv. Mater.* **2012**, *24*, 4041.
[22] W. Y. Wu, J. N. Schulman, T. Y. Hsu, U. Efron, *Appl. Phys. Lett.* **1987**, *51*, 710.
[23] A. Roshko, T. E. Harvey, B. L. Hyland, S. Y. Lehman, K. D. Cobry, *J. Cryst. Growth* **2009**, *311*, 4109.
[24] G. S. Solomon, *Appl. Phys. Lett.* **2004**, *84*, 2073.
[25] Y. Lou, J. L. Bassani, *J. Mech. Phys. Solids* **2008**, *56*, 3507.
[26] S. Aggarwal, A. P. Monga, S. R. Perusse, R. Ramesh, V. Ballarotto, E. D. Williams, B. R. Chalamala, Y. Wei, R. H. Reuss, *Science* **2000**, *287*, 2235.
[27] J. L. MacManus-Driscoll, S. R. Foltyn, Q. X. Jia, H. Wang, A. Serquis, L. Civale, B. Maiorov, M. E. Hawley, M. P. Maley, D. E. Peterson, *Nat. Mater.* **2004**, *3*, 439.
[28] S. Kang, A. Goyal, J. Li, A. A. Gapud, P. M. Martin, L. Heatherly, J. R. Thompson, D. K. Christen, F. A. List, M. Paranthaman, D. F. Lee, *Science* **2006**, *311*, 1911.
[29] J. Gutiérrez, A. Llordés, J. Gázquez, M. Gibert, N. Romà, S. Ricart, A. Pomar, F. Sandiumenge, N. Mestres, T. Puig, X. Obradors, *Nat. Mater.* **2007**, *6*, 367.
[30] B. Maiorov, S. A. Baily, H. Zhou, O. Ugurlu, J. A. Kennison, P. C. Dowden, T. G. Holesinger, S. R. Foltyn, L. Civale, *Nat. Mater.* **2009**, *8*, 398.
[31] S. H. Wee, Y. Gao, Y. L. Zuev, K. L. More, J. Meng, J. Zhong, G. M. Stocks, A. Goyal, *Adv. Funct. Mater.* **2013**, *23*, 1912.
[32] C. Cantoni, Y. Gao, S. H. Wee, E. D. Specht, J. Gazquez, J. Meng, S. J. Pennycook, A. Goyal, *ACS Nano* **2011**, *6*, 4783.
[33] H. Yang, H. Wang, B. Maiorov, J. Lee, D. Talbayev, M. J. Hinton, D. M. Feldmann, J. L. MacManus-Driscoll, A. J. Taylor, L. Civale, T. R. Lemberger, Q. X. Jia, *J. Appl. Phys.* **2009**, *106*, 093914.
[34] F. J. Baca, T. J. Haugan, P. N. Barnes, T. G. Holesinger, B. Maiorov, R. Lu, X. Wang, J. N. Reichart, J. Z. Wu, *Adv. Funct. Mater.* **2013**, *23*, 4826.
[35] P. Mele, K. Matsumoto, A. Ichinose, M. Mukaida, Y. Yoshida, S. Horii, R. Kita, *Supercond. Sci. Technol.* **2008**, *21*, 125017.
[36] A. Augieri, G. Celentano, V. Galluzzi, A. Mancini, A. Rufoloni, A. Vannozzi, A. A. Armenio, T. Petrisor, L. Ciontea, S. Rubanov, E. Silva, N. Pompeo, *J. Appl. Phys.* **2010**, *108*, 063906.
[37] P. Mikheenko, V. S. Dang, Y. Y. Tse, M. A. Kechik, P. Paturi, H. Huhtinen, Y. Wang, A. Sarkar, J. S. Abell, A. Crisan, *Supercond. Sci. Technol.* **2010**, *23*, 125007.
[38] A. Xu, J. J. Jaroszynski, F. Kametani, Z. Chen, D. C. Larbalestier, Y. L. Viouchkov, Y. Chen, Y. Xie, V. Selvamanickam, *Supercond. Sci. Technol.* **2010**, *23*, 014003.
[39] J. Jestin, F. Cousin, I. Dubois, C. Ménager, R. Schweins, J. Oberdisse, F. Boué, *Adv. Mater.* **2008**, *20*, 2533.
[40] G. Belingardi, E. G. Koricho, A. T. Beyene, *Composite Structures* **2013**, *102*, 237.
[41] A. Silhanek, L. Civale, S. Candia, G. Nieva, *Phys. Rev. B* **1999**, *59*, 13620.
[42] P. Vukusic, J. R. Sambles, *Nature* **2003**, *424*, 852.
[43] J. Huang, X. Wang, Z. L. Wang, *Nano. Lett.* **2006**, *6*, 2325.
[44] T. Lenau, M. Barfoed, *Adv. Eng. Mater.* **2008**, *10*, 299.
[45] V. Saranathan, C. O. Osuji, S. G. J. Mochrie, H. Noh, S. Narayanan, A. Sandy, E. R. Dufresne, R. O. Prum, *Proc. Natl. Acad. Sci. USA* **2010**, *107*, 11676.
[46] D. Zhu, C. F. Ortega, R. Motamedi, L. Szewciw, F. Vernerey, F. Barthelat, *Adv. Biomater.* **2012**, *14*, B185.
[47] M. Varela, Z. Sefrioui, D. Arias, M. A. Navacerrada, M. Lucía, M. A. López de la Torre, C. León, G. D. Loos, F. Sánchez-Quesada, J. Santamaría, *Phys. Rev. Lett.* **1999**, *83*, 3936.
[48] S. R. Foltyn, L. Civale, J. L. MacManus-Driscoll, Q. X. Jia, B. Maiorov, H. Wang, M. Maley, *Nat. Mater.* **2007**, *6*, 631.
[49] R. Round, B. Bridge, *J. Mater. Sci. Lett.* **1987**, *6*, 1471.
[50] P. Baumgart, S. Blumenröder, A. Erle, B. Hillebrands, G. Güntherodt, H. Schmidt, *Solid State Commu.* **1989**, *69*, 1135.
[51] P. Baumgart, S. Blumenröder, A. Erle, B. Hillebrands, P. Splittgerber, G. Güntherodt, H. Schmidt, *Physica C* **1989**, *162*, 1073.
[52] P. Terki, H. Feraoun, G. Bertrand, H. Aourag, *Phys. Stat. Sol. (b)* **2005**, *242*, 1054.
[53] J. L. MacManus-Driscoll, J. A. Alonso, P. C. Wang, T. H. Geballe, J. C. Bravman, *Physica C* **1994**, *232*, 288.
[54] S. C. Wimbush, M. Li, M. E. Vickers, B. Maiorov, D. M. Feldmann, Q. X. Jia, J. L. MacManus-Driscoll, *Adv. Funct. Mater.* **2009**, *19*, 835.
[55] H. Yang, H. Wang, J. Yoon, Y. Wang, M. Jain, D. M. Feldmann, P. C. Dowden, J. L. MacManus-Driscoll, Q. X. Jia, *Adv. Mater.* **2009**, *21*, 3794.
[56] S. A. Harrington, J. Zhai, S. Denev, V. Gopalan, H. Wang, Z. Bi, S. A. T. Redfern, S. H. Baek, C. W. Bark, C. B. Eom, Q. X. Jia, M. E. Vickers, J. L. MacManus-Driscoll, *Nat. Nanotechnol.* **2011**, *6*, 491.